Structural comparison of the C-terminal domain of functionally divergent lyssavirus P proteins

Aoi Sugiyama[1], Tomo Nomai[2], Xinxin Jiang[2], Miku Minami[1], Min Yao[1], Katsumi Maenaka[2], Naoto Ito[3], Paul R. Gooley[4], Gregory W. Moseley[5], and Toyoyuki Ose*[1, 2, 6]

[1]Faculty of Advanced Life Science, [2]Faculty of Pharmaceutical Sciences, Hokkaido University, Kita-12, Nishi-6, Kita-ku, Sapporo 060-0812, Japan; [3]Faculty of Applied Biological Sciences, Gifu University, 1-1 Yanagido, Gifu 501-1193, Japan; [4]Department of Biochemistry and Molecular Biology, University of Melbourne, Parkville, Victoria 3010, Australia; [5]Department of Microbiology, Biomedicine Discovery Institute, Monash University, Clayton Campus, Victoria 3800, Australia; [6]PRESTO, Japan Science and Technology Agency, Chiyoda-ku, Tokyo 102-8666, Japan.

*To whom correspondence should be addressed: Toyoyuki Ose
ose.toyoyuki@sci.hokudai.ac.jp;

ABSTRACT

Lyssavirus P protein is a multifunctional protein that interacts with numerous host-cell proteins. The C-terminal domain (CTD) of P is important for inhibition of JAK-STAT signaling enabling the virus to evade host immunity. Several regions on the surface of rabies virus P are reported to interact with host factors. Among them, an extended, discrete hydrophobic patch is notable. Although structures of the C-terminal domain of P proteins of two strains of rabies virus, and of mokola virus have been solved, the structure for Duvenhage virus P, which is functionally divergent from these species for immune evasion function, is not known. Here, we analyze the structures of the C-terminal domains of P of Duvenhage and of a distinct rabies virus strain to gain further insight on the nature and potential function of the hydrophobic surface. Molecular contacts in crystals suggest that the hydrophobic patch is important to intermolecular interactions with other proteins, which differ between the lyssavirus species.

1. Introduction

Rabies is a zoonotic disease with a case-fatality rate of almost 100% to humans in non-vaccinated individuals [1]. In the *Lyssavirus* genus (family *Rhabdoviridae*), that comprises the causative agents of rabies, seven major species have been categorized including rabies virus (RABV, genotype 1); Lagos bat virus (genotype 2); Mokola virus (MOKV, genotype 3); Duvenhage virus (DUVV, genotype 4); European bat lyssaviruses type 1 and 2 (EBLV, genotypes 5 and 6); and Australian bat lyssavirus (genotype 7) [2]. Lyssaviruses have a nonsegmented, negative-stranded RNA genome encoding five proteins; N (nucleoprotein), P (phosphoprotein), M (matrix protein), G (glycoprotein), and L (large protein) [3]. Studies have shown that RABV infects humans most commonly through bites from infected dogs. RABV is responsible for about 60,000 death every year, mainly in Asia and Africa [4] despite availability of effective vaccines. Current vaccines only protect against phylogroup I lyssaviruses, but more divergent lyssaviruses have caused human deaths with the relative burden of non-RABV lyssavirus infections likely to be underestimated [5].

Lyssavirus P consists of a long-disordered N-terminal region (amino acids 1-90 (numbering corresponds to RABV Nishigahara strain)), a central dimerization domain (DD, amino acids 91-133), a disordered linker (amino acids 134-185), followed by a C-terminal domain (CTD, amino acids 185-297). P is a multifunctional protein which

contains a large number of host-protein binding sites as well as sites for binding to viral proteins. P binds to nascent RNA-free nucleoprotein (N) protein using the first 60 N terminal residues and prevents N protein from binding non-specifically to cellular RNA [6]. P is required as a cofactor of large protein (L), which is composed of two RNA-dependent RNA polymerase subunits [7]. Viral transcription and replication also rely on the binding to the N/RNA complex *via* the C-terminal domain (CTD) of P [8]. In the N-terminal region of P, residues 11-50 were identified to be sufficient to stimulate the processivity of L as the RNA polymerase [9]. P interacts with a wide variety of host proteins such as the dynein light chain LC8 [10,11], microtubules (MT) [12], ribosomal protein L9 [13], mitochondrial complex I [14], IRF-3 [15], STAT [16,17], promyelocytic leukaemia (PML) protein nuclear bodies [18], nuclear import/export receptors [19] and nucleolin [20].

The interferon (IFN) system, including type I (primarily IFN α/β) and II (IFN γ) which are critical to the development of innate and adaptive immune responses against viral infection, is targeted by many pathogenic viruses, *via* proteins called interferon (IFN) antagonists [21]. STAT molecules are common targets of many viral interferon (IFN) antagonists, including those of lyssaviruses, flaviviruses, influenza virus, and paramyxoviruses [22]. Because of a lack of complex structural information, the details of the interactions between viral proteins and STATs remain largely unknown. To the best of our knowledge, the N-terminal domain of STAT1 with C-protein of Sendai virus is the only crystal structure of a STAT in complex with a viral protein [23]. However, we recently examined in detail the interaction between RABV-P CTD and unphosphorylated human STAT1 (U-STAT1), and mapped important residues on the RABV-P CTD surface [24]. Using transferred cross-saturation NMR, we revealed that three regions on P-CTD termed region A (Ile201-Fhe209), region B (Asp235-: Lys237), and region C (Leu276-Val277) form an extended interface for STAT1 binding (Fig. 1). Mutagenesis and cell assays suggested that the regions A and B were critical for binding with the region of STAT1 containing the coiled-coil domain (CCD) and DNA-binding domain (DBD), whereas region C contributes to an interaction involving the N- and/or C-terminal domains [24]. Conversely, Trp265 and Met287, previously indicated by mutagenesis to be important for STAT1 antagonism by RABV CVS strain P protein (CVS-P), and by Nishigahara (Ni)-P in recombinant virus [25] and transfected protein [24], appeared not to be directly involved in binding to STAT1 [24]. These residues have been of interest

since crystal structures of RABV-P (CVS-P and Pasteur vaccine strain (PV)-P) and MOKV-P CTD identified a unique hydrophobic pocket (the "W-hole") within which the residues reside [25–27]. Trp265 is not conserved in all lyssaviruses; although RABV, Australian bat lyssavirus (ABLV), Aravan virus (ARAV) and Khujand virus (KHUV) have tryptophan and MOKV and Lagos bat virus (LBV) share the bulky hydrophobic phenylalanine, Shimoni bat virus (SHIV) and West Caucasian virus (WCV) and Ikoma lyssavirus (IKOV) have tyrosine, it is substituted for glycine in DUVV, EBLV2, and Irkut virus (IRKV) (Fig. 1) and a serine in EBLV1. Notably, while STAT1 binding/antagonism is broadly conserved among a number of lyssavirus P proteins with the Trp or Phe at the position 265, DUVV P displays moderately reduced antagonistic function compared with RABV P, and introduction of W265-G mutation to RABV P results in a similar defect [25,28]. Thus, while the W-hole does not contact U-STAT1, it impacts STAT1 binding, but the specific mechanistic basis of this is unknown. Viral STAT antagonists often have many targets and data from P protein indicates that STAT1 binding can involve multipoint interactions [24]. Here, we determine the crystal structure of DUVV-P CTD, which naturally contains G at Trp265 and so can be used to assess function/significance as a 'surrogate' for mutated RABV P protein, which is unstable as a recombinant protein. We also describe the crystal structure of RABV Nishigaraha strain P-CTD (Ni-P CTD) containing a K214A substitution, but which retains the bulky tryptophan (Trp265) at the center of the extensive hydrophobic pocket. Lys214, a residue comprising part of a positive patch on RABV-P CTD, was suggested to be important for interacting with N protein from X-ray SAXS analysis [29] and genome replication assay [25], as well as in nuclear import [30] although structural analysis of effects of mutation of this residue has not been reported. These two new P-CTD structures enable us to compare the effects of the bulky hydrophobic side chains at the hydrophobic pocket.

2. Materials and methods

Methods for protein expression, purification, crystallization and CD spectroscopy are provided in supplementary materials.

X-ray data of Ni-P CTD K214A were collected at the beamline NE3A of Photon Factory Advanced Ring (Tsukuba, Japan). The data set was integrated, merged, and scaled using XDS [31] and aimless [32]. Diffraction data of DUVV-P CTD were

collected at the beamline BL45XU of SPring-8 (Hyogo, Japan). The automated data collection system ZOO [33] was used, and all the datasets were merged, integrated, and scaled to 1.95 Å using the KAMO system [34], which exploits BLEND [32], XDS [31], and XSCALE [35]. Briefly, a 20 μm^2 beam was exposed to each crystal over 10-degree rotation with a total radiation dose of 10 MGy. One frame of the diffraction images was obtained from 0.1˚ crystal rotation with a frame rate of 50 Hz. After clustering by BLEND, 59 data sets from 10 different crystal conditions were merged and scaled for structure determination (4 crystals from JCSG II #18, 12 crystals from JCSG III #11, 7 crystals from PEGs # 44, 3 crystals from PEGs #46, one crystal from PEGs #47, 12 crystals from PEGs II suite #16, 2 crystals from PEGs II suite #80, 5 crystals from classics suite #44, 2 crystals from classics suite #61, 11 crystals from classics suite #72).

The structures of Ni-P CTD K214A and DUVV-P CTD were solved by the molecular replacement method using the program Molrep [32]. The crystal structure of CVS-P CTD (PDBID: 1VYI) was used as a search model. Structure refinement was done using Refmac5 [32] and Phenix [36]. Details of the data collection and processing statistics are given in Table 1.

3. Results

3.1 RABV-P (Nishigahara strain) CTD K214A structure

The region composed of 102 residues of Ni-P CTD K214A covering amino acid 194 - 295 was built and refined using 3.0 Å diffracted data. The overall structure shows the same morphology previously described as resembling a half pear, with a flat and curved face [26,27] (Fig. 2). The amino acids are well conserved in the reported CVS-P CTD (PDBID, 1VYI) [26], and PV-P CTD structures (3OA1); 4 residues are different between Ni-P CTD and CVS-P CTD (257, 281, 284, and 295) and between Ni-P CTD and PV-P CTD (223, 252, 280, and 295), respectively (Fig. 1). The root means square distance (RMSD) values between Ni-P CTD and CVS-P CTD, is 0.56 Å, between Ni-P CTD and PV-P CTD, is 0.41 Å, using 102 residues respectively. Thus, there seems no effect of K214A mutations on the overall structure; notably, K214 mutation to alanine was reported to affect P protein trafficking suggesting roles in forming a nuclear localization sequence [30]; the lack of apparent misfolding shown here supports a specific role. Furthermore, this structure can be used for comparison with the hydrophobic pocket with other lyssavirus P proteins.

3.2 DUVV-P CTD structure

The 2.0 Å resolution crystal structure of the DUVV-P CTD covering amino acid 193 – 297 also revealed a half pear morphology, composed of seven tightly folded α helices, a 3_{10} helix and a small β sheet consisting of two β strands (Fig. 1, 2). The RMSD value of DUVV-P CTD and CVS-P CTD is 0.64 Å using 105 Cα atoms, and that of DUVV-P CTD and MOKV-P CTD (PDBID, 2wzl) is 0.51 Å using 101 Cα atoms. The most striking difference between DUVV-P CTD and RABV-P CTD is seen in the flat face. The bulky side chain, composing part of the unique hydrophobic patch W-hole, typically Trp265 (for example, in RABV-P) or Phe266 (for example, in MOKV-P), is exchanged for a glycine (Gly266) in DUVV-P CTD. Additionally, three continuous polar residues Ser269, Thr270, and His271 on the helix 4 in DUVV-P CTD are substituted for Leu268, Ala269, and Asn270 in RABV (Ni)-P CTD. Consequently, the shape of the hydrophobic pocket differs between DUVV-P CTD and RABV-P CTD (Fig. 2 c - e).

3.3 Comparison of the hydrophobic patch

Around the W-hole, the hydrophobic patch is extensive on the flat face of P-CTD from RABV CVS, PV strain (PDBID, 3OA1), Ni strain K214A (this study), MOKV (2WZL), and DUVV (this study). The K214A site of Ni-P CTD K214A is not used for the comparison here as it has no significant impact on the CTD structure; the structure is used solely for comparison of the hydrophobic patch between proteins. The other residues constructing the extended hydrophobic patch are Val244, Pro245, Leu268, Ala269, Val278, Ala280 (Ser280 in PV strain), Leu283, Met287, and Leu291, are conserved between CTDs of different RABV strains (Fig. 1). Among these, Leu268 and Ala269 are not conserved in DUVV-P CTD, in addition to the non-conserved Trp265. It is interesting to focus on the bulky side chain (Trp265 in RABV or Phe266 in MOKV) at the center of the large hydrophobic region, for comparison between the solved CTD structures. We checked hydrophobic interactions mediated by the hydrophobic patches in crystal packing using the three known and two newly analyzed structures of lyssavirus P-CTD (Fig. 3). In the RABV CVS-P CTD structure, the patch (with Trp265) is used to interact with Trp186 from a neighboring monomer and Phe209, Leu234 from another monomer; in the RABV PV-P CTD structure, the patch (with Trp265) is used to interact with Ala202, Ala206, Phe209, and Leu234 from neighboring monomer; in the RABV Ni-P CTD

structure; the patch (with Trp265) is used to interact with the hydrophobic part of side-chain Lys212 and Leu224 from neighboring monomer. In the MOKV-P CTD structure, the patch (with Phe266) is used to interact with Leu225 and the hydrophobic part of Glu303. However, only in DUVV-P CTD structure with the corresponding residue glycine (Gly266) at the center of the hydrophobic surface, this region is not used for the interaction with other molecules in crystal packing.

3.4 The effect of W265G mutation

The CD spectra of W265G/M287V reported previously indicated that the minimum value is distinctively different from wild type (WT) protein, but components of secondary structure is similar [24]. We also examined the CD spectra of Ni-P CTD W265G. The full CD spectra and estimated secondary structure of Ni-P CTD are similar to WT and W265G with slightly different minima (Fig. 4). The low solubility of W265G or W265G/M287V was reported previously [24]. We also observed instability of purified Ni-P CTD W265G; tendency to get precipitated. Therefore, the establishment of the system to assay the effects on P protein interactions of W265G is important for future work to define the interactions formed by Trp265.

4. Discussion

Using purified proteins, we recently showed the potentially complex nature of RABV-P CTD/STAT1 interactions [24]. The regions important for binding with U-STAT1 (A, B, and C) (Fig. 1) are extensively located over the surface of RABV-P CTD but exclude the hydrophobic patch of which Trp265 is located at the center (Fig. 2). Trp265 and Met287 were previously suggested to be important for STAT1 antagonism [25]. Double mutations of RABV-P CTD (W265G/M287V) were later shown to cause significant instability of the protein folding, possibly resulting in the impact on the function of RABV-P CTD [24]. The effect of the single mutation W265G on RABV-P CTD to the overall structure and the interaction with STAT1 remains to be explained, and is significant given that this is a naturally occurring difference in several lyssavirus species. Here, we successfully solved the crystal structure of DUVV-P CTD, which can be considered a ‘surrogate’ for the mutated RABV-P CTD W265G. The shape of the hydrophobic patch on the flat side on the surface is significantly different from that of RABV-P CTD (Fig. 2). Because hydrophobic surfaces on protein molecules tend to

engage in favorable interactions, we compared the contribution of the hydrophobic patch to contact neighboring molecules in the crystals. Surprisingly, among all of the solved P-CTD structures of lyssavirus, in P-CTD structures with bulky side chains at the 265 position (Trp or Phe; RABV (CVS, PV, Ni) and MOKV), the hydrophobic pocket is used to stabilize the crystal packings. In the case of DUVV-P CTD with glycine at the corresponding position, the hydrophobic patch is not used for any intermolecular interactions. Results of IFN-dependent luciferase reporter assays in previous study [24] showed that Ni-P containing W265G mutation reduces IFN-dependent luciferase induction to ~12% of that observed for a standard control (CVS PΔ30) entirely deficient in STAT1 targeting [24], although it was still defective compared with CVS-P WT or Ni-P WT (both of which inhibit luciferase expression to ~3% of that for the control). The partial defect caused by W265G is consistent with the fact that this mutation did not appear to not directly interact with U-STAT1; however, the fact that W265G effects a significant defect compared to wild-type proteins [24,25] indicates that it is likely to impact on interactions with other molecular species such as phosphorylated STAT1 or other proteins, formed by Trp265 within the W-hole.

Acknowledgments

We thank N. Matsugaki and Y. Yamada for assistance in data collection at Photon Factory. We also thank K. Hirata, N. Sakai, and Y. Nakamura for the guidance of auto-data collection at SPring-8. CD spectra measurements were carried out in the courtesy of T. Aizawa. This work was supported in part by the Japan Society for the Promotion of Science KAKENHI (Grants 17K07296). This research was also supported by the Platform Project for Supporting Drug Discovery and Life Science Research funded by Japan AMED and Hokkaido University, and the Global Facility Center and Pharma Science Open Unit funded by MEXT under “Support Program for Implementation of New Equipment Sharing System”.

Figure legends

Fig. 1 Multiple sequence alignment for the CTD of Lyssavirus P-proteins

Alignment (Clustal Omega) was performed for P-CTDs of RABV Ni (Nishigahara strain, SWISSPROTdb Q9IPJ8), RABV CVS (CVS strain, P22363), RABV Pasteur (Pasteur vaccine strain (PV), P06747), MOKV (Mokola virus, P0C569), EBLV1 (European bat lyssavirus 1, A4UHP9), EBLV2 (European bat lyssavirus 2, A4UHQ4), IRKV (Irkut virus, Q5VKP5), ARAV (Aravan virus, Q6X1D7), KHUV (Khujand virus, Q6X1D3), MOKV (Mokola virus, P0C569), LBV (Lagos bat virus, O56773), and DUVV (Duvenhage virus, O56774). Structures reported are shown with PDBIDs. Secondary structures of RABV Ni-P CTD and DUVV-P CTD from this work are shown at the top and the bottom of the sequence respectively. η indicates a 3_{10} helix. Amino acids conserved completely are highlighted in red with white letters; conserved partially are indicated as red letters. Regions A, B, C, reported previously to be important for the interaction with unphosphorylated STAT1, and the typical tryptophan position at the center of the W-hole are indicated in blue.

Fig. 2

Structure comparison of P-CTDs from the same angle.

(*a*) Structure superimposition of P-CTD of RABV Ni K214A (Nishigahara (Ni) strain, light blue) and RABV CVS (CVS strain, yellow). Residues of Ni-P CTD composing the hydrophobic patch are denoted with stick model. (*b*) Structure superimposition of P-CTD of DUVV (magenta) and RABV CVS (CVS strain, yellow) with secondary structure labeling. Side chains of four residues in the hydrophobic patch withe are not conserved in two proteins were shown as stick models. Labeling of the residues: CVS-P/DUVV-P. (*c* - *e*) Surface representation of P-CTD with hydrophobicity; the extent is indicated by green color darkness. The surface of RABV CVS-P CTD (c), RABV Ni-P CTD K214A (d), and DUVV-P CTD (e) are shown with positions of the residue corresponding to "tryptophan" of W-hole (residue 265 in RABV).

Fig. 3

Contribution of the W-hole for interaction with neighboring monomers in crystal packings. The hydrophobic surfaces are indicated as Fig.2. Hydrophobic moieties of interacting partners are shown as gray stick models with main chain traces. P-CTDs of (a) RABV CVS, (b) RABV Pasteur vaccine (PV) strain, (c) RABV Ni K214A, and (d) MOKV are shown.

Fig. 4

CD spectra of RABV Ni-P CTD WT (solid line) and W265G (dotted line).

Table 1

Data collection and refinement statistics

	Ni-P CTD K214A (PDBID, 7C20)	DUVV-P CTD WT (PDBID, 7C21)
Data Collection		
Space group	$P4_12_12$	$C2$
Cell dimensions		
(Å, ˚)	$a = b = 51.27$, $c = 90.11$	$a = 95.19$, $b = 49.52$, $c = 25.28$, $\beta = 99.75$
Resolution (Å)[a]	45.0 - 3.0 (3.29- 3.0)	43.8 -1.95 (2.07- 1.95)
R_{meas}	0.158 (0.635)	0.216 (1.385)
$I/\sigma I$	5.0 (3.0)	7.53 (1.56)
CC1/2	0.998(0.947)	0.99 (0.607)
Completeness (%)	100 (100)	98.0 (97.4)
Redundancy	13.6 (14.7)	8.6 (8.6)
Wilson B-factor	47.16	23.57
Refinement		
Resolution (Å)	36.25 - 3.0 (3.11- 3.0)	43.8 - 1.95 (2.14 - 1.95)
No. reflections	2683 (254)	8366 (2060)
R_{work}/R_{free}	0.2073 (0.3362) /0.2587 (0.3463)	0.1980 (0.2150) /0.2645 (0.3007)
No. atoms		
Protein	806	840
Solvent	0	52
B-factors		
Protein	32.43	26.80
R.m.s deviations		
Bond lengths (Å)	0.002	0.007
Bond angles (˚)	1.55	0.83
Ramachandran Plot (%)		
Favored	97	99.03
Allowed	3	0
outliers	0	0.97

[1] D.L. Knobel, S. Cleaveland, P.G. Coleman, E.M. Fèvre, M.I. Meltzer, M.E.G. Miranda, A. Shaw, J. Zinsstag, F.-X. Meslin, Re-evaluating the burden of rabies in Africa and Asia, Bull World Health Organ. 83 (2005) 360–368.

[2] J.S. Evans, D.L. Horton, A.J. Easton, A.R. Fooks, A.C. Banyard, Rabies virus vaccines: is there a need for a pan-lyssavirus vaccine?, Vaccine 30 (2012) 7447–7454, doi:10.1016/j.vaccine.2012.10.015.

[3] O. Delmas, E.C. Holmes, C. Talbi, F. Larrous, L. Dacheux, C. Bouchier, H. Bourhy, Genomic diversity and evolution of the lyssaviruses, Plos One 3 (2008) e2057, doi:10.1371/journal.pone.0002057.

[4] K. Hampson, L. Coudeville, T. Lembo, M. Sambo, A. Kieffer, M. Attlan, J. Barrat, J.D. Blanton, D.J. Briggs, S. Cleaveland, P. Costa, C.M. Freuling, E. Hiby, L. Knopf, F. Leanes, F.-X. Meslin, A. Metlin, M.E. Miranda, T. Müller, L.H. Nel, S. Recuenco, C.E. Rupprecht, C. Schumacher, L. Taylor, M.A.N. Vigilato, J. Zinsstag, J. Dushoff, G.A. for R.C.P. for R. Prevention, Estimating the global burden of endemic canine rabies, Plos. Neglect. Trop. D. 9 (2015) e0003709, doi:10.1371/journal.pntd.0003709.

[5] C.R. Fisher, D.G. Streicker, M.J. Schnell, The spread and evolution of rabies virus: conquering new frontiers, Nat. Rev. Microbiol. 16 (2018) 241–255, doi:10.1038/nrmicro.2018.11.

[6] M. Mavrakis, S. Méhouas, E. Réal, F. Iseni, D. Blondel, N. Tordo, R.W.H. Ruigrok, Rabies virus chaperone: Identification of the phosphoprotein peptide that keeps nucleoprotein soluble and free from non-specific RNA, Virology 349 (2006) 422–429, doi:10.1016/j.virol.2006.01.030.

[7] M. Chenik, M. Schnell, K.K. Conzelmann, D. Blondel, Mapping the interacting domains between the rabies virus polymerase and phosphoprotein, J. Virol. 72 (1998) 1925–1930.

[8] C. Leyrat, R. Schneider, E.A. Ribeiro, F. Yabukarski, M. Yao, F.C.A. Gérard, M.R. Jensen, R.W.H. Ruigrok, M. Blackledge, M. Jamin, Ensemble Structure of the Modular and Flexible Full-Length Vesicular Stomatitis Virus Phosphoprotein, J. Mol. Biol. 423 (2012) 182–197, doi:10.1016/j.jmb.2012.07.003.

[9] B. Morin, B. Liang, E. Gardner, R.A. Ross, S.P.J. Whelan, An In Vitro RNA Synthesis Assay for Rabies Virus Defines Ribonucleoprotein Interactions Critical for Polymerase Activity, J. Virol. 91 (2016) e01508-16, doi:10.1128/jvi.01508-16.

[10] Y. Jacob, H. Badrane, P.-E. Ceccaldi, N. Tordo, Cytoplasmic Dynein LC8 Interacts with Lyssavirus Phosphoprotein, J. Virol. 74 (2000) 10217–10222, doi:10.1128/jvi.74.21.10217-10222.2000.

[11] H. Raux, A. Flamand, D. Blondel, Interaction of the Rabies Virus P Protein with the LC8 Dynein Light Chain, J. Virol. 74 (2000) 10212–10216, doi:10.1128/jvi.74.21.10212-10216.2000.

[12] A. Brice, D.R. Whelan, N. Ito, K. Shimizu, L. Wiltzer-Bach, C.Y. Lo, D. Blondel, D.A. Jans, T.D.M. Bell, G.W. Moseley, Quantitative Analysis of the Microtubule Interaction of Rabies Virus P3 Protein: Roles in Immune Evasion and Pathogenesis, Sci. Rep-Uk. 6 (2016) 33493, doi:10.1038/srep33493.

[13] Y. Li, W. Dong, Y. Shi, F. Deng, X. Chen, C. Wan, M. Zhou, L. Zhao, Z.F. Fu, G. Peng, Rabies virus phosphoprotein interacts with ribosomal protein L9 and affects rabies virus replication, Virology 488 (2016) 216–224, doi:10.1016/j.virol.2015.11.018.

[14] W. Kammouni, H. Wood, A. Saleh, C.M. Appolinario, P. Fernyhough, A.C. Jackson, Rabies virus phosphoprotein interacts with mitochondrial Complex I and induces mitochondrial dysfunction and oxidative stress, J. Neurovirol. 21 (2015) 370–382, doi:10.1007/s13365-015-0320-8.

[15] M.K. Chelbi-Alix, A. Vidy, J.E. Bougrini, D. Blondel, Rabies Viral Mechanisms to Escape the IFN System: The Viral Protein P Interferes with IRF-3, Stat1, and PML Nuclear Bodies, J. Interf. Cytokine Res. 26 (2006) 271–280, doi:10.1089/jir.2006.26.271.

[16] A. Vidy, M. Chelbi-Alix, D. Blondel, Rabies Virus P Protein Interacts with STAT1 and Inhibits Interferon Signal Transduction Pathways, J. Virol. 79 (2005) 14411–14420, doi:10.1128/jvi.79.22.14411-14420.2005.

[17] K.G. Lieu, A. Brice, L. Wiltzer, B. Hirst, D.A. Jans, D. Blondel, G.W. Moseley, The rabies virus interferon antagonist P protein interacts with activated STAT3 and inhibits Gp130 receptor signaling, J. Virol. 87 (2013) 8261–8265, doi:10.1128/jvi.00989-13.

[18] D. Blondel, T. Regad, N. Poisson, B. Pavie, F. Harper, P.P. Pandolfi, H. de Thé, M.K. Chelbi-Alix, Rabies virus P and small P products interact directly with PML and reorganize PML nuclear bodies, Oncogene 21 (2002) 7957–7970, doi:10.1038/sj.onc.1205931.

[19] S. Oksayan, L. Wiltzer, C.L. Rowe, D. Blondel, D.A. Jans, G.W. Moseley, A novel nuclear trafficking module regulates the nucleocytoplasmic localization of the rabies virus interferon antagonist, P protein, J. Biol. Chem. 287 (2012) 28112–28121, doi:10.1074/jbc.m112.374694.

[20] S. Oksayan, J. Nikolic, C.T. David, D. Blondel, D.A. Jans, G.W. Moseley, Identification of a role for nucleolin in rabies virus infection., J. Virol. 89 (2015) 1939–43. doi:10.1128/jvi.03320-14.

[21] M.D. Audsley, G.W. Moseley, Paramyxovirus evasion of innate immunity: Diverse strategies for common targets, World. J. Virol. 2 (2013) 57–70, doi:10.5501/wjv.v2.i2.57.

[22] I. Najjar, R. Fagard, STAT1 and pathogens, not a friendly relationship, Biochimie 92 (2010) 425–444, doi:10.1016/j.biochi.2010.02.009.

[23] K. Oda, Y. Matoba, T. Irie, R. Kawabata, M. Fukushi, M. Sugiyama, T. Sakaguchi, Structural Basis of the Inhibition of STAT1 Activity by Sendai Virus C Protein, J. Virol. 89 (2015) 11487–11499, doi:10.1128/jvi.01887-15.

[24] Md.A. Hossain, F. Larrous, S.M. Rawlinson, J. Zhan, A. Sethi, Y. Ibrahim, M. Aloi, K.G. Lieu, Y.-F. Mok, M.D.W. Griffin, N. Ito, T. Ose, H. Bourhy, G.W. Moseley, P.R. Gooley, Structural Elucidation of Viral Antagonism of Innate Immunity at the STAT1 Interface, Cell Reports. 29 (2019) 1934-1945.e8, doi:10.1016/j.celrep.2019.10.020.

[25] L. Wiltzer, K. Okada, S. Yamaoka, F. Larrous, H.V. Kuusisto, M. Sugiyama, D. Blondel, H. Bourhy, D.A. Jans, N. Ito, G.W. Moseley, Interaction of Rabies Virus P-Protein With STAT Proteins is Critical to Lethal Rabies Disease, J. Infect. Dis. 209 (2013) 1744–1753, doi:10.1093/infdis/jit829.

[26] M. Mavrakis, A.A. McCarthy, S. Roche, D. Blondel, R.W.H. Ruigrok, Structure and Function of the C-terminal Domain of the Polymerase Cofactor of Rabies Virus, J. Mol. Biol. 343 (2004) 819–831, doi:10.1016/j.jmb.2004.08.071.

[27] R. Assenberg, O. Delmas, J. Ren, P.-O. Vidalain, A. Verma, F. Larrous, S.C. Graham, F. Tangy, J.M. Grimes, H. Bourhy, Structure of the nucleoprotein binding domain of Mokola virus phosphoprotein., J. Virol. 84 (2009) 1089–1096, doi:10.1128/jvi.01520-09.

[28] L. Wiltzer, F. Larrous, S. Oksayan, N. Ito, G.A. Marsh, L.F. Wang, D. Blondel, H. Bourhy, D.A. Jans, G.W. Moseley, Conservation of a unique mechanism of immune evasion across the Lyssavirus genus., J. Virol. 86 (2012) 10194–10199, doi:10.1128/jvi.01249-12.

[29] E. de A. Ribeiro, C. Leyrat, F.C.A. Gérard, A.A.V. Albertini, C. Falk, R.W.H. Ruigrok, M. Jamin, Binding of Rabies Virus Polymerase Cofactor to Recombinant Circular Nucleoprotein–RNA Complexes, J. Mol. Biol. 394 (2009) 558–575, doi:10.1016/j.jmb.2009.09.042.

[30] D. Pasdeloup, N. Poisson, H. Raux, Y. Gaudin, R.W.H. Ruigrok, D. Blondel, Nucleocytoplasmic shuttling of the rabies virus P protein requires a nuclear localization signal and a CRM1-dependent nuclear export signal, Virology 334 (2005) 284–293, doi:10.1016/j.virol.2005.02.005.

[31] W. Kabsch, XDS, Acta Crystallogr. Sect. D Biol. Crystallogr. 66 (2010) 125–132, doi:10.1107/s0907444909047337.

[32] M.D. Winn, C.C. Ballard, K.D. Cowtan, E.J. Dodson, P. Emsley, P.R. Evans, R.M. Keegan, E.B. Krissinel, A.G.W. Leslie, A. McCoy, S.J. McNicholas, G.N. Murshudov, N.S. Pannu, E.A. Potterton, H.R. Powell, R.J. Read, A. Vagin, K.S. Wilson, Overview of the CCP4 suite and current developments, Acta Crystallogr. Sect. D Biol. Crystallogr. 67 (2011) 235–242, doi:10.1107/s0907444910045749.

[33] K. Hirata, K. Yamashita, G. Ueno, Y. Kawano, K. Hasegawa, T. Kumasaka, M. Yamamoto, ZOO: an automatic data-collection system for high-throughput structure analysis in protein microcrystallography, Acta Crystallogr. Sect. D Biol. Crystallogr. 75 (2019) 138–150, doi:10.1107/s2059798318017795.

[34] K. Yamashita, K. Hirata, M. Yamamoto, KAMO : towards automated data processing for microcrystals, Acta Crystallogr. Sect. D Biol. Crystallogr. 74 (2018) 441–449, doi:10.1107/s2059798318004576.

[35] W. Kabsch, Integration, scaling, space-group assignment and post-refinement., Acta Crystallogr. Sect. D Biol. Crystallogr. 66 (2010) 133–144, doi:10.1107/s0907444909047374.

[36] P.V. Afonine, R.W. Grosse-Kunstleve, N. Echols, J.J. Headd, N.W. Moriarty, M. Mustyakimov, T.C. Terwilliger, A. Urzhumtsev, P.H. Zwart, P.D. Adams, Towards automated crystallographic structure refinement with phenix.refine, Acta Crystallogr. Sect. D Biol. Crystallogr. 68 (2012) 352–367, doi:10.1107/s0907444912001308.

Fig. 1

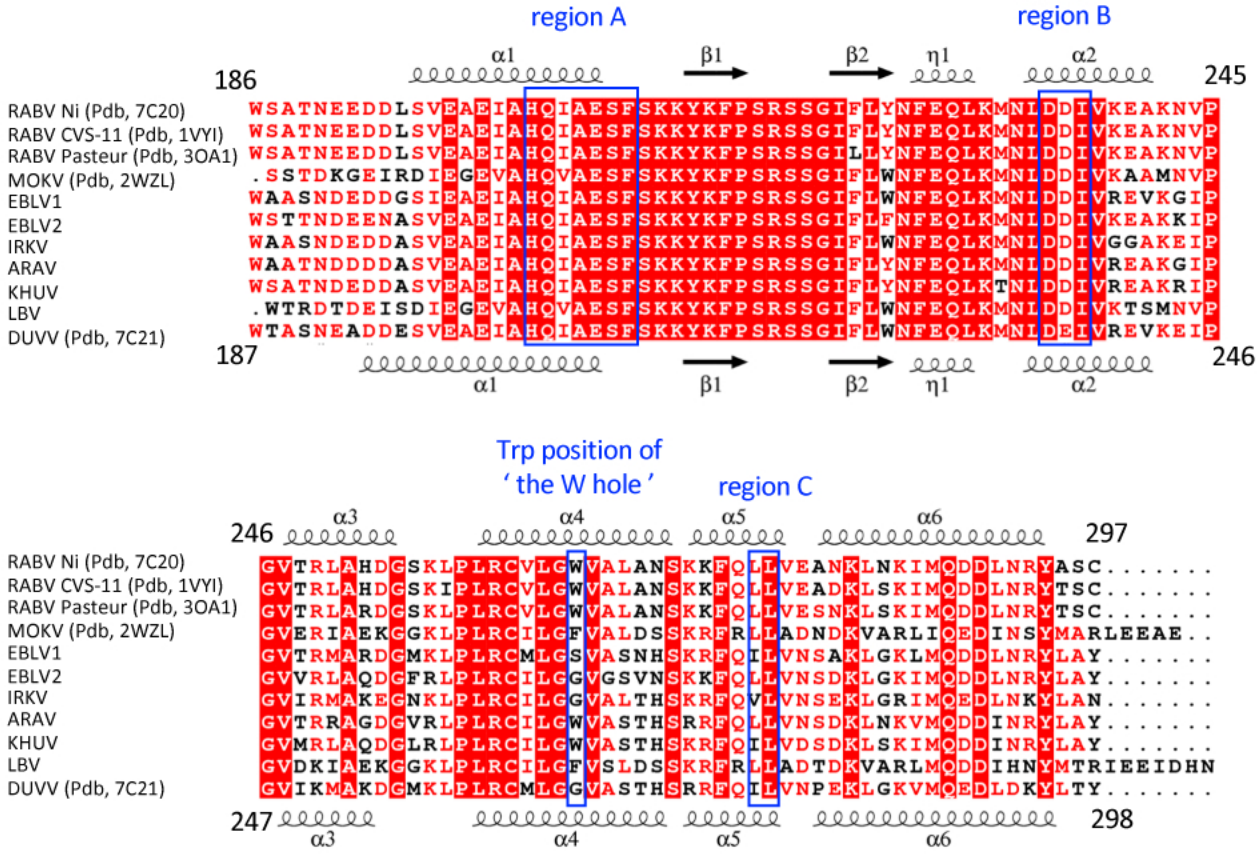
region A
region B
α1
β1
β2
η1
α2
186
245
RABV Ni (Pdb, 7C20)
RABV CVS-11 (Pdb, 1VYI)
RABV Pasteur (Pdb, 3OA1)
MOKV (Pdb, 2WZL)
EBLV1
EBLV2
IRKV
ARAV
KHUV
LBV
DUVV (Pdb, 7C21)
187
246
Trp position of
' the W hole '
region C
α3
α4
α5
α6
246
297
247
298

Fig. 2

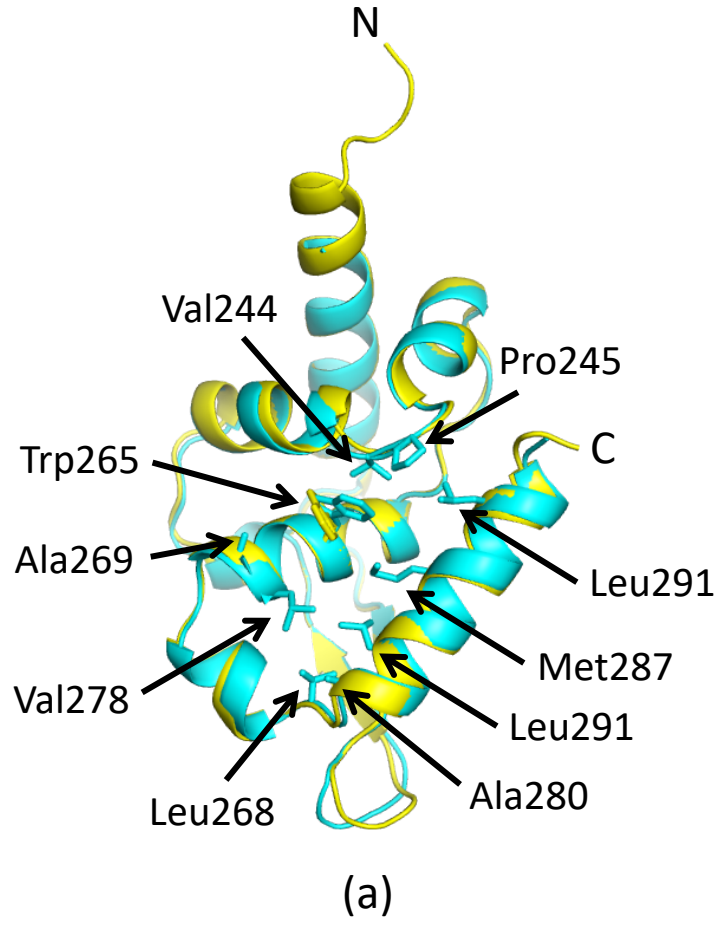
N
Val244
Pro245
C
Trp265
Ala269
Leu291
Met287
Val278
Leu291
Ala280
Leu268

(a)

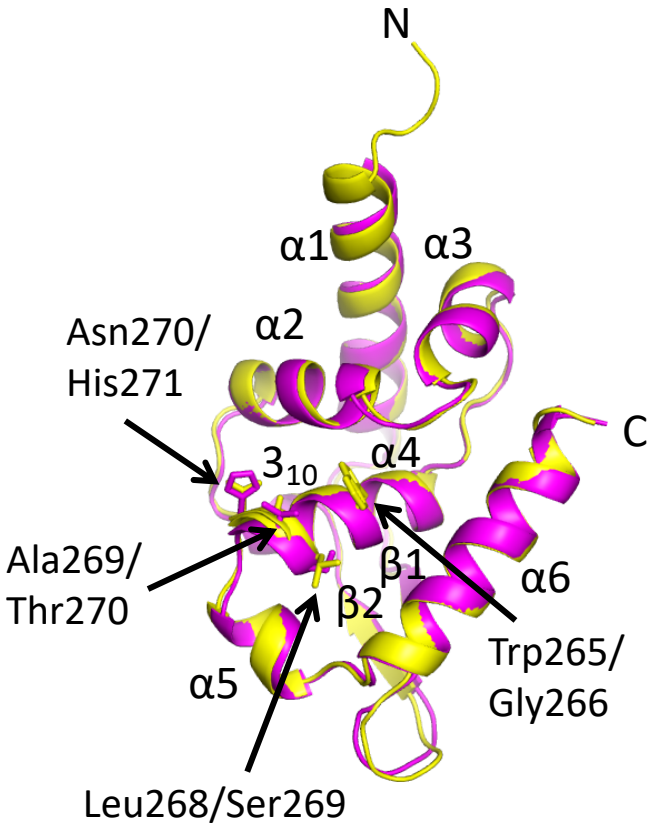
N
α1
α3
Asn270/
His271
α2
C
3₁₀
α4
Ala269/
Thr270
β1
α6
β2
Trp265/
Gly266
α5
Leu268/Ser269

(b)

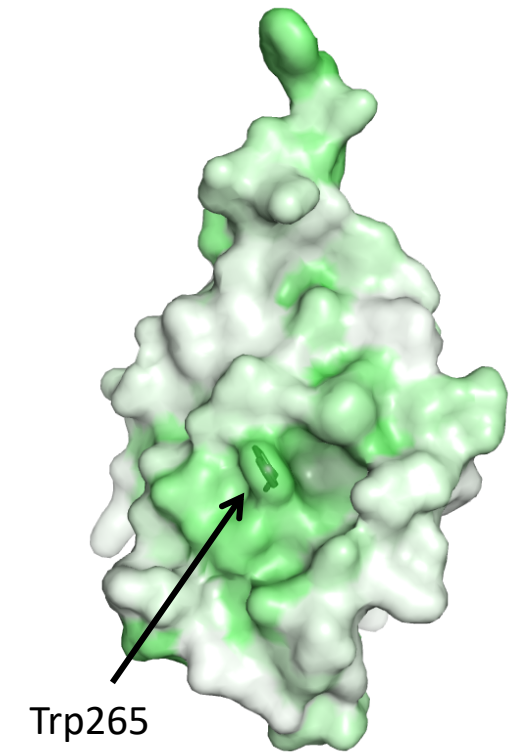
Trp265

(c)

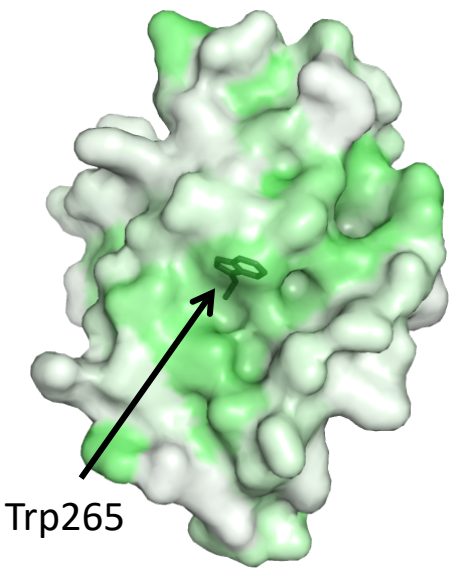
Trp265

(d)

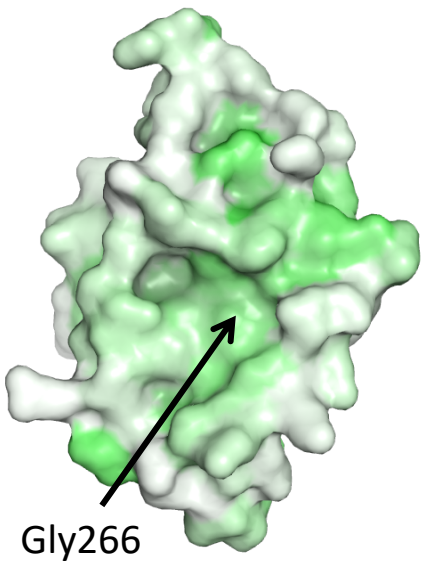
Gly266

(e)

Fig. 3

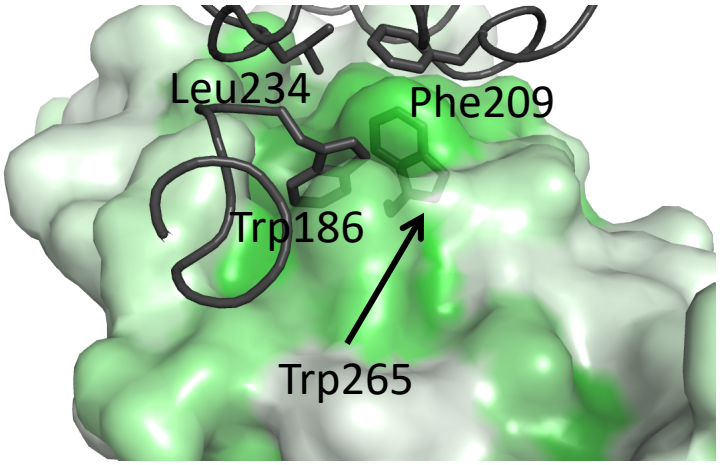

(a) CV-P CTD

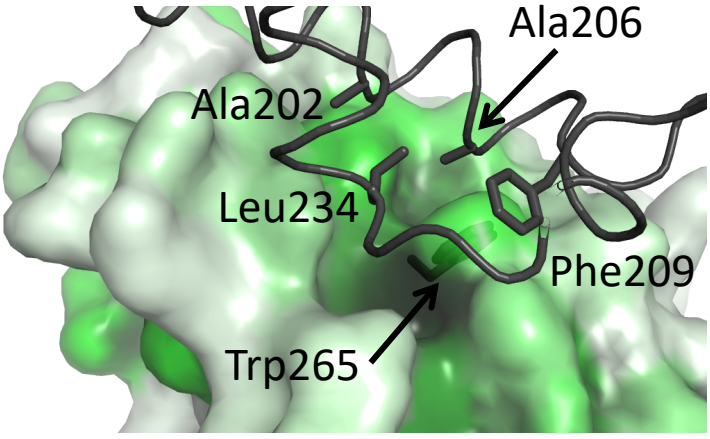

(b) PV-P CTD

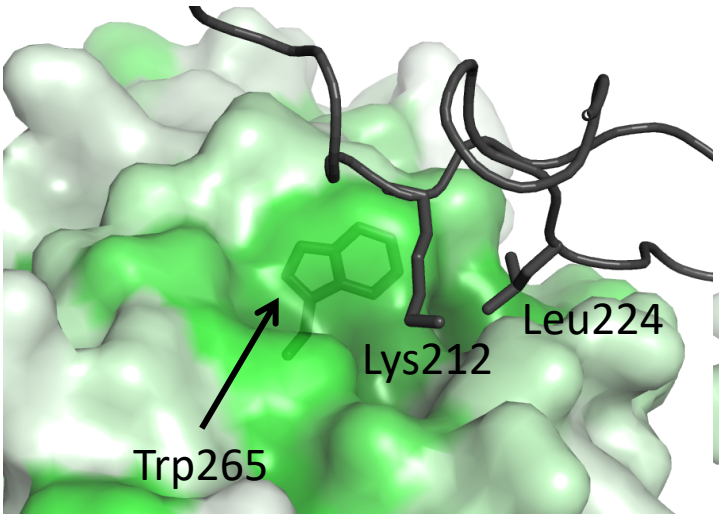

(c) Ni-P CTD

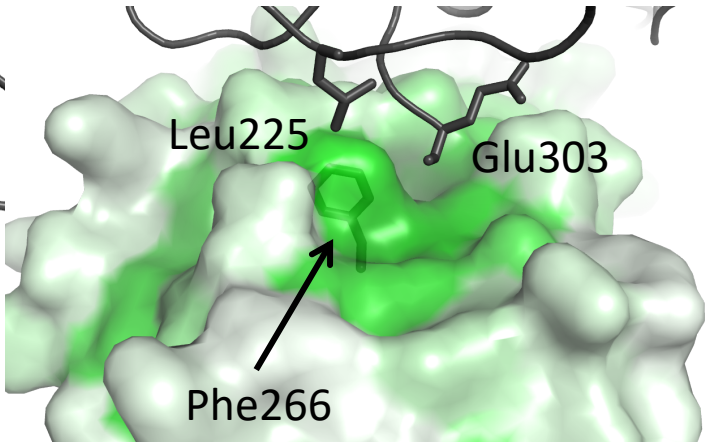

(d) MOKV-P CTD

Fig. 4

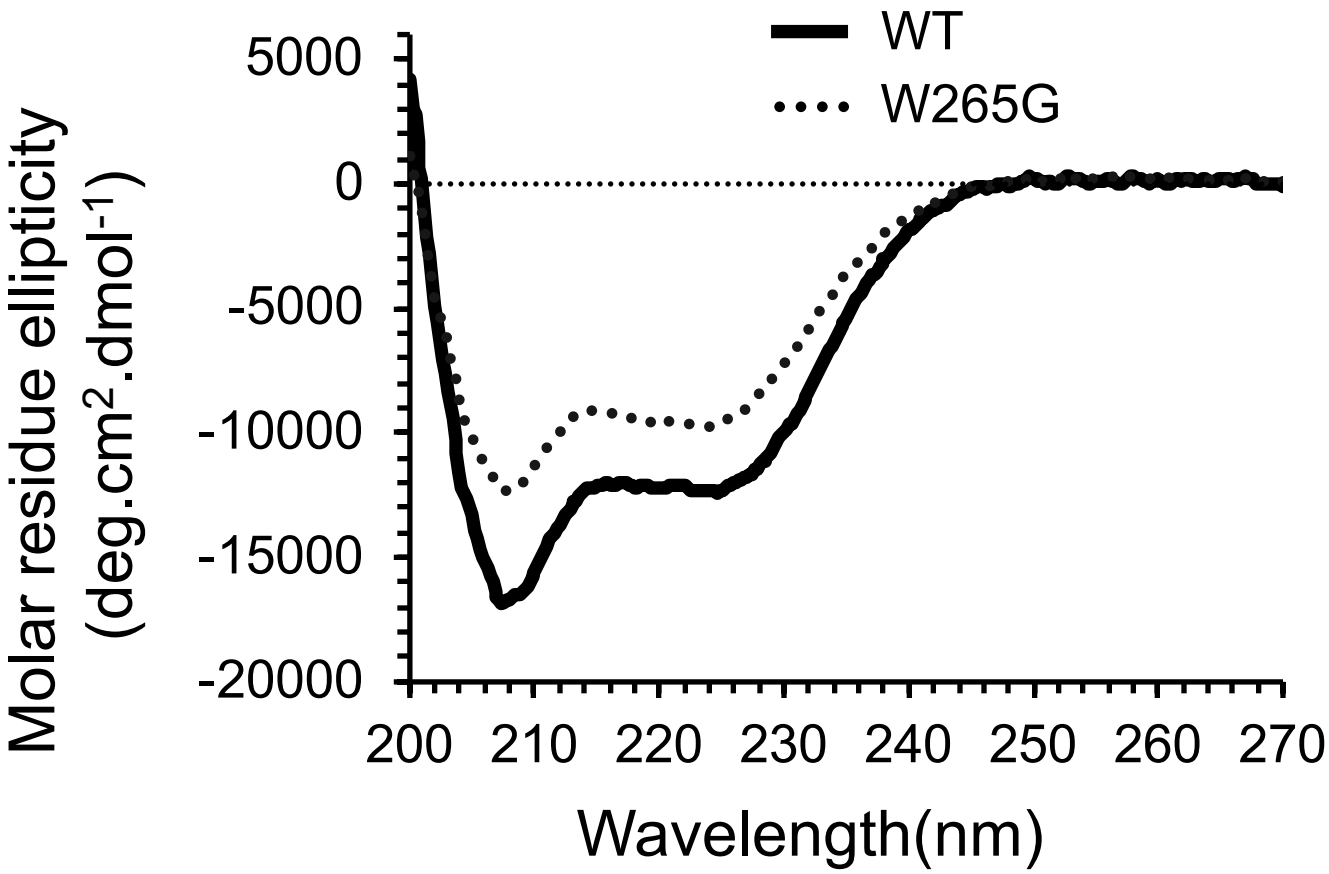
WT
W265G
5000
0
-5000
-10000
-15000
-20000
200
210
220
230
240
250
260
270
Molar residue ellipticity
(deg.cm2.dmol-1)
Wavelength(nm)